

Analysis of band structures of phosphorene and bismuthene based on the double group theory

メタデータ	言語: eng 出版者: 公開日: 2022-03-04 キーワード (Ja): キーワード (En): 作成者: メールアドレス: 所属:
URL	https://doi.org/10.24517/00065538

This work is licensed under a Creative Commons Attribution-NonCommercial-ShareAlike 3.0 International License.



REGULAR PAPER • OPEN ACCESS

Analysis of band structures of phosphorene and bismuthene based on the double group theory

To cite this article: Muhammad Yusuf Hakim Widiyanto and Mineo Saito 2022 *Jpn. J. Appl. Phys.* **61** 035503

View the [article online](#) for updates and enhancements.

You may also like

- [Realization of versatile electronic, magnetic properties and new topological phases in hydrogenated bismuthene](#)
Ming-Yang Liu, Qing-Yuan Chen, Chao Cao et al.
- [Tunable electronic properties in bismuthene/2D silicon carbide van der Waals heterobilayer](#)
Joy D. Sarker, Md. Sherajul Islam, Naim Ferdous et al.
- [Anisotropic thermoelectric effect on phosphorene and bismuthene: first-principles calculations based on nonequilibrium Green's function theory](#)
Yuto Tanaka, Mineo Saito and Fumiyuki Ishii



Analysis of band structures of phosphorene and bismuthene based on the double group theory

Muhammad Yusuf Hakim Widiyanto* and Mineo Saito

Faculty of Mathematics and Physics, Institute of Science and Technology, Kanazawa University, Kanazawa 920-1192, Japan

*E-mail: mwidiyanto@cphys.s.kanazawa-u.ac.jp

Received September 29, 2021; revised December 24, 2021; accepted January 16, 2022; published online March 3, 2022

We study band structures of group-V two-dimensional materials, i.e. phosphorene and bismuthene, by carrying out first-principles calculations including spin-orbit coupling (SOC). We propose a method to identify irreducible representations (IR) of both symmorphic and nonsymmorphic systems. We find for the α structures that all the non-SOC bands are doubly degenerated on the first Brillouin zone edge due to sticking or pairing of bands and that the SOC slightly splits the bands in most of the cases. We evaluate Z_2 invariants based on identified IR. We find that the Z_2 invariant of 1 in the case of β bismuthene is due to the strong SOC that reverses the highest occupied and the lowest unoccupied bands at the Γ point. © 2022 The Author(s). Published on behalf of The Japan Society of Applied Physics by IOP Publishing Ltd

1. Introduction

Group-V two-dimensional materials have been attracting scientific interest for over the past decade. Whereas electronic structures of group-IV two-dimensional materials are characterized by the Dirac cone,¹⁻³⁾ group-V two-dimensional materials are semiconductors and are suitable for applications to thermoelectrics, spintronics and optoelectronics devices.⁴⁻⁸⁾

It was found for ultrathin Bi films on the Si (111) surface that films form puckered (α) structures when the thickness is very small and the six-member ring (β) structure becomes stable when the thickness becomes large.⁹⁻¹¹⁾ Since Bi is a heavy atom, the spin-orbit coupling (SOC) greatly affects the electronic structures of the films which are now called bismuthene. For example, the Rashba effect and the possibility of the topological insulators have been studied.¹²⁻¹⁷⁾ The SOC also affects the thermoelectric effect.⁶⁾

A theoretical study on phosphorene predicted that the band gap decreases and becomes close to that of the black phosphorous as thickness increases.¹⁸⁾ Later, phosphorene was really achieved experimentally and it was confirmed that the band gap is higher than that of the black phosphorous; the band gaps are in the range from 0.3 eV to 2.0 eV.¹⁹⁻²²⁾ Optical and electronic properties, in particular, attract scientific interests. Furthermore, the possibility of a Dirac metal and a topological insulator for bilayers was discussed.^{23,24)}

To deeply understand electronic structures, we need to analyze band structures based on the group theory. Since the SOC plays an important role in the spintronics application of group-V two-dimensional materials, it is necessary to clarify the IR of bands based on the double group theory. However, little is known about IR for these materials.

In this paper, we study α and β structures of phosphorene and bismuthene and identify IR of bands calculated from the first-principles method. Since α structures are nonsymmorphic, we study the sticking of the non-SOC bands and the split of the stuck bands due to the SOC. We also analyze the pairing of bands induced by the time-reversal symmetry. We evaluate Z_2

invariants in the systems having inversion symmetry based on the analysis of identified IR.

2. Method

The function of identifying IR was implemented in some first-principles codes.²⁵⁻²⁹⁾ We also reported methods for the non-SOC calculations³⁰⁻³⁴⁾ and for the SOC calculations on symmorphic systems.³⁵⁾ We here report the method for nonsymmorphic systems.

The two-component spinor Bloch wavefunction is expressed as:

$$\Psi_{\mathbf{k},n} = \begin{pmatrix} \psi_{\mathbf{k},n}^{\alpha} \\ \psi_{\mathbf{k},n}^{\beta} \end{pmatrix}, \quad (1)$$

where \mathbf{k} is the wavevector in the first Brillouin zone and n is the band index in the ascending order of energy. The two spin-dependent wavefunctions are given by:

$$\psi_{\mathbf{k},n}^{\alpha(\beta)}(\mathbf{r}) = \frac{1}{\sqrt{NV}} \sum_u c_{\mathbf{k},n}^{\alpha(\beta)}(\mathbf{G}_u) \exp[i(\mathbf{k} + \mathbf{G}_u) \cdot \mathbf{r}], \quad (2)$$

where N is the number of unit cells and V is the unit cell volume. \mathbf{G}_u and $c_n^{\alpha(\beta)}(\mathbf{G}_u)$ are the u -th reciprocal lattice vector and a coefficient, respectively.

We evaluate the following expression to identify the IR of the Bloch wave functions which have the b -th degeneracy:

$$Q^\gamma = \frac{1}{l} \sum_{n=a}^{a+b-1} \sum_j \chi^\gamma(\hat{R}_j)^* \langle \Psi_{\mathbf{k},n} | \hat{R}_j | \Psi_{\mathbf{k},n} \rangle, \quad (3)$$

where l is the order of the group and $\chi^\gamma(\hat{R}_j)$ is the character of IR γ . j runs over the symmetry operations, \hat{R}_j , of the k -group, which are represented by Seitz notation, $\hat{R}_j = \{\hat{\Theta}_j | \tau_j\}$, where $\hat{\Theta}_j$ and τ_j represent rotation and fractional translation, respectively. When $Q^\gamma = 1$ ($Q^\gamma = 0$), the wave functions belong (do not belong) to the γ -th IR.



By combining Eqs. (1)–(3), we get:

$$Q^\gamma = \frac{1}{l} \sum_{n=a}^{a+b-1} \sum_j \sum_u X^\gamma(\hat{R}_j)^* \times \exp(-i(\hat{\Theta}_j \mathbf{G}_u - \mathbf{G}'_j) \cdot \boldsymbol{\tau}_j) [c_{\mathbf{k},n}^\alpha(\hat{\Theta}_j \mathbf{G}_u - \mathbf{G}'_j)^* \times [M_{11}^j c_{\mathbf{k},n}^\alpha(\mathbf{G}_u) + M_{12}^j c_{\mathbf{k},n}^\beta(\mathbf{G}_u)] + c_{\mathbf{k},n}^\beta(\hat{\Theta}_j \mathbf{G}_u - \mathbf{G}'_j) * [M_{21}^j c_{\mathbf{k},n}^\alpha(\mathbf{G}_u) + M_{22}^j c_{\mathbf{k},n}^\beta(\mathbf{G}_u)]] \quad (4)$$

where the reciprocal lattice vector \mathbf{G}'_j satisfies $\hat{\Theta}_j \mathbf{k} = \mathbf{k} - \mathbf{G}'_j$ ($\mathbf{G}'_j = 0$ when the k -point is located inside the first Brillouin zone). In the above expression, we introduce the ray representation whose character is given by:

$$X^\gamma(\hat{R}_j) = \chi^\gamma(\hat{R}_j) \exp(i\mathbf{k} \cdot \boldsymbol{\tau}_j). \quad (5)$$

Hereafter we simply call this ray representation IR. The matrix \mathbf{M}^j represents the rotation (\hat{R}_j) for spin functions, α and β :

$$\begin{bmatrix} M_{11}^j & M_{12}^j \\ M_{21}^j & M_{22}^j \end{bmatrix} = \begin{bmatrix} \cos(\varphi_j/2) - iv_j \sin(\varphi_j/2) & -i(\lambda_j - i\mu_j) \sin(\varphi_j/2) \\ -i(\lambda_j + i\mu_j) \sin(\varphi_j/2) & \cos(\varphi_j/2) + iv_j \sin(\varphi_j/2) \end{bmatrix}, \quad (6)$$

where φ_j is the rotation angle around the axis whose direction cosine is (λ_j, μ_j, v_j) .³⁶⁾

We apply the above mentioned method to plane-wave base calculations, i.e. the ultrasoft pseudopotential³⁷⁾ and projector augmented wave (PAW) calculations.³⁸⁾ We apply Eq. (4) to the soft (plane-wave) part after the part is normalized. Since the soft part itself belongs to IR, the calculated Q^γ in Eq. (4) is close to an integer value (0 or 1).

Density functional theory (DFT) band structure calculations are carried out based on the generalized gradient approximation.³⁹⁾ First-principles calculation code PHASE/O⁴⁰⁾ is used for these calculations. Ultrasoft and PAW methods are applied to non-SOC and SOC calculations. We use slab models to simulate two-dimensional materials; a vacuum space around 20 Å in the z direction is introduced to avoid interaction between interlayers. The k -point mesh is $30 \times 30 \times 1$ for both structures.

3. Results and discussion

3.1. Geometry optimization

The unit cell of α and β structures are defined in Fig. 1 and the first Brillouin zone is shown in Fig. 2. We consider the two cases for the α structures, i.e. buckled and non-buckled structures. The former and latter belong to $Pmn2_1(C_{2v}^7)$ and $Pmna(D_{2h}^7)$, respectively.³⁰⁾

The β structure belongs to $P\bar{3}m1(D_{3d}^3)$, which is the same as the space group of buckled group-IV two-dimensional materials.³²⁾ The non-buckled α structure and β one have the inversion symmetry and we locate the origin at the inversion symmetry point as shown in Fig. 1.

We optimize the lattice constants and atomic positions of α and β structures by using DFT calculations (Table I). The bond lengths and bond angles of phosphorene obtained from SOC calculations are close to those from non-SOC calculations. The bond lengths and bond angles are found to vary within 0.001 Å and 0.1°. On the other hand, there is a small

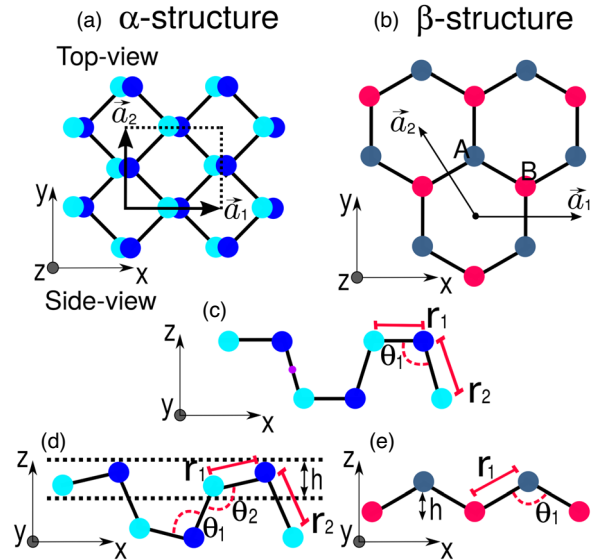


Fig. 1. (Color online) Atomic structures. Top views of the (a) α and (b) β structures and side views of the (c) non-buckled α , (d) buckled α , and (e) β structures are presented. The original points are located at the inversion symmetry points. The original point of the α structure is located at the bond center which is indicated by the purple point in (c) whereas the original point of the β structure is located at the center of the six-member ring as shown in (b).

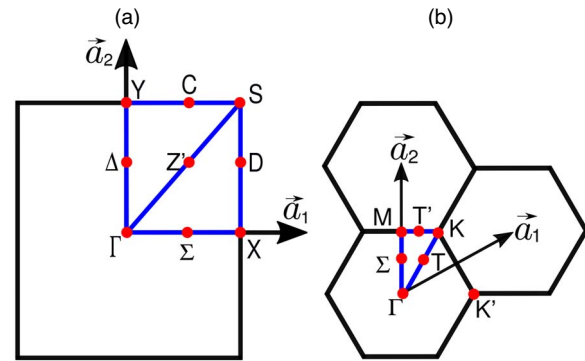


Fig. 2. (Color online) Brillouin zone of the (a) α and (b) β structures. \vec{a}_1 and \vec{a}_2 are the primitive reciprocal lattice vectors.

difference between the geometries optimized from non-SOC and SOC calculations for bismuthene. The bond lengths and bond angles vary within 0.06 Å and 0.3° (Table I).

α phosphorene and α bismuthene are found to form non-buckled and buckled structures, respectively. The buckling height of bismuthene is evaluated as 0.52 Å by using the SOC calculation. This buckling is due to electron transfer from the high-position atom to the low-position atom.^{6,18,30)} The low-position atom has slightly higher partial density of states (PDOS) than the high-position atom for the occupied band near the Fermi energy and vice versa for the unoccupied band near the Fermi energy. These results indicate the electron transfer from the high position atom to the low position atom [Figs. 3(a) and 3(b)].

3.2. Group theoretical analysis of α and β structures

The IR for the k point groups are well established and we use Bethe⁴¹⁾ and Mulliken symbols^{42,43)} to represent the IR. We call these IR *conventional* IR in this paper. In the case of Mulliken symbols for the double group, we use notations of a

Table I. Calculated α and β structures. The lattice constants (a_1 and a_2), bond lengths (r_1 and r_2), buckling height (h) and bond angles (θ_1 and θ_2) are defined in Fig. 1. The units of the bond angles are degrees. The results of non-SOC calculations are in the parentheses.

Systems	a_1 (Å)	a_2 (Å)	r_1 (Å)	r_2 (Å)	h (Å)	θ_1	θ_2
α phosphorene	4.52 (4.52)	3.38 (3.38)	2.24 (2.24)	2.25 (2.25)	—	102.8 (102.8)	—
β phosphorene	3.27 (3.27)	—	2.26 (2.26)	—	1.24 (1.24)	92.8 (92.6)	—
α bismuthene	4.84 (4.88)	4.49 (4.41)	3.08 (3.07)	3.04 (2.98)	0.52 (0.54)	84.9 (84.8)	104.6 (104.9)
β bismuthene	4.30 (4.26)	—	3.03 (3.02)	—	1.72 (1.72)	90.3 (89.8)	—

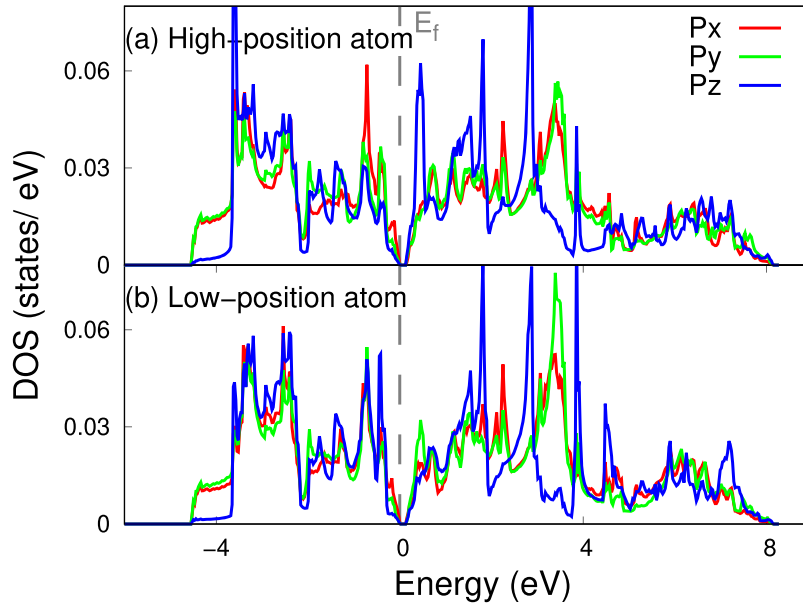


Fig. 3. (Color online) PDOS of (a) high-position and (b) low-position atoms in buckled α bismuthene calculated by including the SOC. The energy is measured from the valence band top.

reference.⁴⁴ The symbols used in this study are the same as those in a textbook.³⁶

It is well known that the IR are different from the above-mentioned conventional ones on some or all of the first Brillouin zone edge (FBZE) in nonsymmorphic systems.³⁶ We call these IR *unconventional* IR in this paper. We introduce overlines for the unconventional IR symbols to distinguish them from the conventional Bethe symbols (Table II). As explained later, the unconventional IR induces sticking of non-SOC bands and the SOC splits the bands in most cases.

A pair of bands belonging to different IR have the same energy in some cases. This pairing due to time-reversal symmetry is identified by evaluating the Herring sum^{34,45} (see Table III).

3.2.1. α structures. We first study α phosphorene by carrying out non-SOC calculations. The IR of the bands at the k -points except for the FBZE (X-S-Y lines) are conventional and these IR are represented by Mulliken symbols in Fig. 4(a). These bands belong to one-dimensional IR and are not energetically degenerated. On the other hand, all the bands are degenerated on the FBZE. This degeneracy originates from the *sticking* of two bands, which is intrinsic to FBZE in nonsymmorphic systems: The stuck two bands belong to two-dimensional IR which are different from conventional IR.^{30,31} The character tables for these unconventional IR have been reported in a previous paper³⁰ and

these unconventional IR are represented by overlined numbers in the band figure in Fig. 4(a).

We now study the SOC band structure of α phosphorene [Fig. 4(b)]. Since this system has the inversion symmetry, all the bands are degenerated due to time-reversal symmetry, i.e. Kramers pairing occurs. We find that the stuck (doubly degenerated) bands on the FBZE in the non-SOC calculation split into two Kramers pairs on the D-S-C line [Fig. 4(b)]. On this line, SOC four bands belong to different one-dimensional unconventional IR and two of the four are paired due to the time-reversal symmetry. For example, the four bands at the S points belong to \overline{S}_1^\pm , \overline{S}_2^\pm , \overline{S}_3^\pm and \overline{S}_4^\pm and the \overline{S}_1^\pm (\overline{S}_3^\pm) and \overline{S}_2^\pm (\overline{S}_4^\pm) are paired as Table III shows (The overline notation (\overline{S}_n^\pm) is used to represent unconventional IR as explained in the previous Sect. 3.2 and the characters are tabulated in Table II).

The above-mentioned splits of the SOC bands on the D-S-C line are found to be very small. The split of the highest occupied band has the maximum at the S point and the maximum value is 22 meV, which is close to those in previous calculations.^{46,47}

The SOC does not split the bands at the X and Y points, i.e. four bands have the same energy. At the X (Y) points, two Kramers pairs belonging to different unconventional two-dimensional IR, \overline{X}_1 and \overline{X}_2 (\overline{Y}_1 and \overline{Y}_2), have the same energy due to the time-reversal symmetry (Table III).

Table II. Character table of the unconventional IR for SOC bands of the α structures. The following symmetry operations are presented; $E = \{E|0\}$, $C_{2x} = \{C_{2x}|\tau\}$, $C_{2y} = \{C_{2y}|0\}$, $C_{2z} = \{C_{2z}|\tau\}$, $I = \{I|0\}$, $\sigma_{yz} = \{\sigma_{yz}|\tau\}$, $\sigma_{xz} = \{\sigma_{xz}|0\}$, and $\sigma_{xy} = \{\sigma_{xy}|\tau\}$, where $\tau = \frac{1}{2}\mathbf{a}_1 + \frac{1}{2}\mathbf{a}_2$. \mathbf{a}_1 and \mathbf{a}_2 are primitive lattice vectors defined in Fig. 2.

Non-buckled										Buckled						
k -point	IR	E	C_{2x}	C_{2y}	C_{2z}	I	σ_{yz}	σ_{xz}	σ_{xy}	k -point	IR	E	C_{2x}	σ_{xz}	σ_{xy}	
X (D_{2h})	\bar{X}_1	2	0	$-2i$	0	0	0	0	0	S (C_{2v})	\bar{S}_1	1	1	$-i$	$-i$	
	\bar{X}_2	2	0	$2i$	0	0	0	0	0		\bar{S}_2	1	1	i	i	
D (C_{2v})	\bar{D}_1	1		$-i$			1		$-i$	Y (C_{2v})	\bar{S}_3	1	-1	$-i$	i	
	\bar{D}_2	1		$-i$		-1		i			\bar{S}_4	1	-1	i	$-i$	
	\bar{D}_3	1		i		1		i			\bar{Y}_1	1	1	$-i$	$-i$	
	\bar{D}_4	1		i		-1		$-i$			\bar{Y}_2	1	1	i	i	
S (D_{2h})	\bar{S}_1^+	1	1	$-i$	$-i$	1	1	$-i$	$-i$	Non-buckled, Buckled	\bar{Y}_3	1	-1	$-i$	i	
	\bar{S}_1^-	1	1	$-i$	$-i$	-1	-1	i	i		\bar{Y}_4	1	-1	i	$-i$	
	\bar{S}_2^+	1	1	i	i	1	1	i	i		k -point					
	\bar{S}_2^-	1	1	i	i	-1	-1	$-i$	$-i$		C (C_{2v})	\bar{C}_1	1	1	$-i$	$-i$
	\bar{S}_3^+	1	-1	$-i$	i	1	-1	$-i$	i			\bar{C}_2	1	1	i	i
	\bar{S}_3^-	1	-1	$-i$	i	-1	1	i	$-i$			\bar{C}_3	1	-1	$-i$	i
	\bar{S}_4^+	1	-1	i	$-i$	1	-1	i	$-i$			\bar{C}_4	1	-1	i	$-i$
	Y (D_{2h})	\bar{Y}_1	2	0	0	0	0	0	$-2i$		0					
\bar{Y}_2		2	0	0	0	0	0	$2i$	0							

Table III. Pairing of SOC bands due to the time-reversal symmetry in the cases of α and β structures, which is checked by evaluating the Herring sum.

System	k -point	Pairing
α (non-buckled)	X (D_{2h})	$\bar{X}_1 \bar{X}_2$
	D (C_{2v})	$\bar{D}_1 \bar{D}_3; \bar{D}_2 \bar{D}_4$
	S (D_{2h})	$\bar{S}_1^+ \bar{S}_3^+; \bar{S}_3^- \bar{S}_4^+$ $\bar{S}_1^- \bar{S}_2^-; \bar{S}_3^- \bar{S}_4^-$
	C (C_{2v})	$\bar{C}_1 \bar{C}_2; \bar{C}_3 \bar{C}_4$
	Y (D_{2h})	$\bar{Y}_1 \bar{Y}_2$
α (buckled)	Z' (C_s)	$e_{1/2}(1) (Z'_3) e_{1/2}(2) (Z'_4)$
	D (C_s)	$e_{1/2}(1) (D_3) e_{1/2}(2) (D_4)$
	S (D_{2h})	$\bar{S}_1 \bar{S}_2; \bar{S}_3 \bar{S}_4$
	Y (D_{2h})	$\bar{Y}_1 \bar{Y}_4; \bar{Y}_2 \bar{Y}_3$
	β	Γ (D_{3d})
K (D_3)		$e_{3/2}(1) (K_4) e_{3/2}(2) (K_5)$
M (C_{2h})		$e_{1/2g}(1) (M_3^+) e_{1/2g}(2) (M_4^+)$ $e_{1/2u}(1) (M_3^-) e_{1/2u}(2) (M_4^-)$
Σ (C_s)		$e_{1/2}(1) (\Sigma_3) e_{1/2}(2) (\Sigma_4)$
T (C_2)		$e_{1/2}(1) (T_3) e_{1/2}(2) (T_4)$

We here carry out non-SOC calculation on α bismuthene [Fig. 4(c)]. All the bands at the whole FBZE are doubly degenerated. The degeneracy on the S-Y line is due to the sticking as in the case of α phosphorene. On the other hand, the bands on the X-D line belong to one-dimensional conventional IR and two IR are paired due to the time-reversal symmetry.

We next carry out SOC calculation [Fig. 4(d)]. This system does not have inversion symmetry in sharp contrast with phosphorene, which has the inversion symmetry leading to the Kramers pairing at all k -points.

We find that the non-SOC stuck bands on the C line split into four bands having different energies and belong to unconventional one-dimensional IR, \bar{C}_1 , \bar{C}_2 , \bar{C}_3 and \bar{C}_4 (Table II). On the other hand, the non-SOC stuck bands at the S and Y points split into two doubly degenerated bands because two of the four bands belong to two different unconventional one-dimensional IR which are paired (Table III).

The SOC splits the non-SOC paired bands on the X-D line into two groups, each of which consists of doubly-degenerated bands. The degeneracy for each group on the D line is due to the pairing, i.e. two different one-dimensional IR $e_{1/2}(1)$ (D_3) and $e_{1/2}(2)$ (D_4) are paired (since the original Mulliken symbols $E_{1/2}$ corresponds to two one-dimensional IR, D_3 and D_4 , we introduce the symbols, $e_{1/2}(1)$ and $e_{1/2}(2)$, to represent D_3 and D_4 , respectively). On the other hand, the SOC doubly degenerated bands at the X point belong to two-dimensional conventional IR, $E_{1/2}$ (X_5).

Overall the splits of the SOC bands are larger than those in phosphorene. For example, the split at the S point (242 meV) is larger than the value in phosphorene (22 meV).

The bands in α bismuthene are doubly degenerated at the Γ point which is a time-reversal-invariant momenta (TRIM). It is well known that the bands split around the Γ point in general when the system does not have the inversion symmetry. Indeed, we find band splits overall around the Γ point but the Σ line is the exception. Since the Σ line belongs to the high symmetry group C_{2v} , all the bands belong to the two-dimensional representation $E_{1/2}(\Sigma_5)$.

We tentatively perform a band structure calculation for the non-buckled bismuthene which has a higher energy than the buckled bismuthene (Fig. 5). We optimize the non-buckled structure by using the unit cell which is the same as that of the buckled structure in Table I and find that the band gap (60 meV) is smaller than that (140 meV) of the buckled structure. The space group belongs to the same that of α phosphorene and all the SOC bands are doubly degenerated due to Kramers pairs since the system has the inversion symmetry.

3.2.2. β structures. We carry out non-SOC calculations on β phosphorene [Fig. 6(a)]. The bands belong to one-dimensional IR except for the bands at the Γ and K points whose symmetry groups are D_{3d} and D_3 , respectively. Since the symmetries are high at these two k -points, the symmetry groups include two-dimensional IR (E , E_g and E_u) which induce doubly degenerated bands. The highest occupied and the lowest unoccupied bands at the Γ point belong to E_g and A_{2u} , respectively.

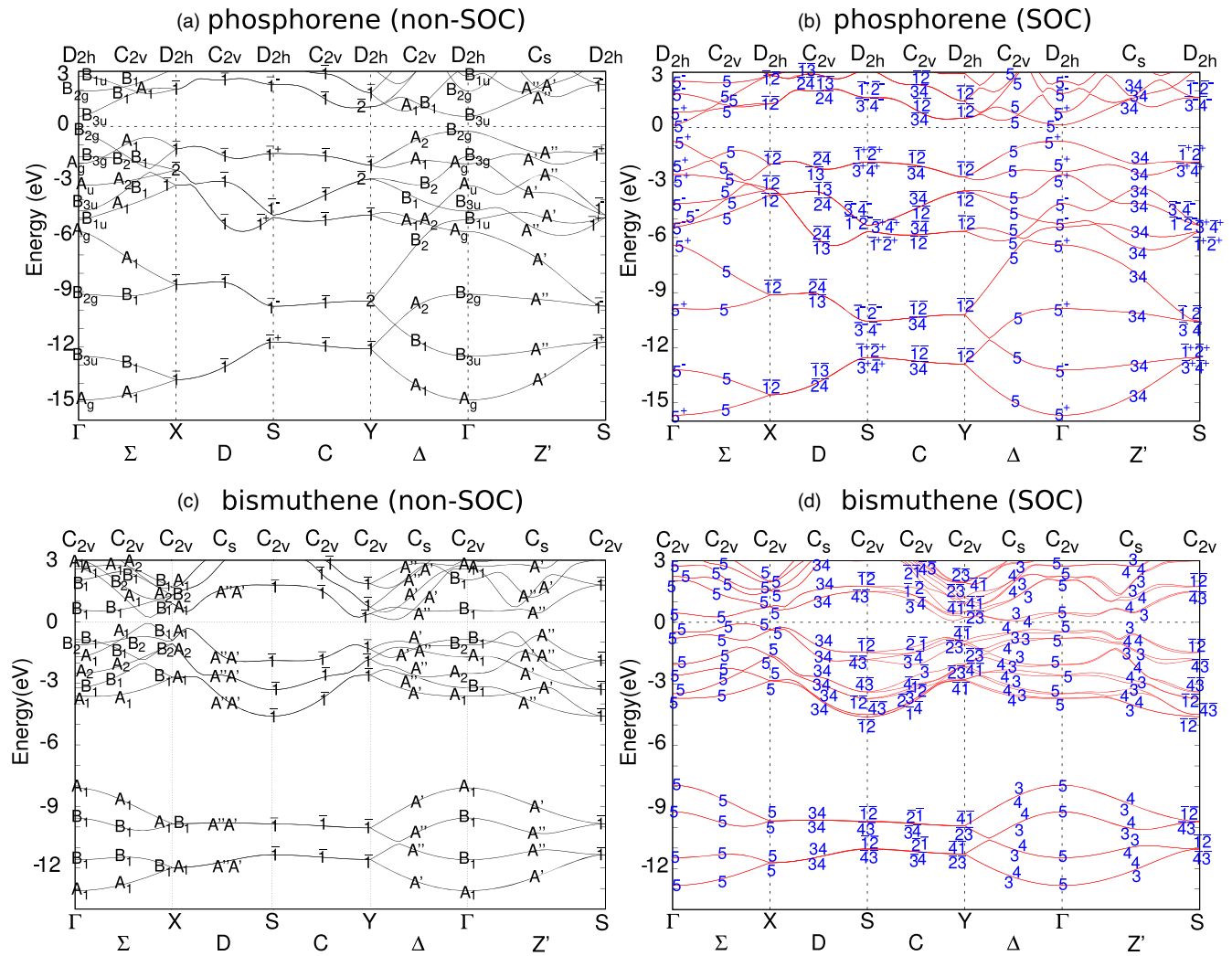


Fig. 4. (Color online) Non-SOC and SOC band structures in the cases of α phosphorene [(a) and (b)] and α bismuthene [(c) and (d)]. In the non-SOC bands, the doubly degenerated unconventional IR are represented by overlined numbers and the conventional IR are represented by Mulliken symbols. In the SOC bands, the conventional IR are represented by numbers which correspond to the subscripts of Bethe symbols. The unconventional IR are represented by overlined numbers and their characters are shown in Table II. The superscript (\pm) indicates the parity. In the case of the phosphorene SOC band, for example, 5 on the Σ line and $\bar{1}^+$ at the S point correspond to Σ_5 and \bar{S}_1^+ , respectively.

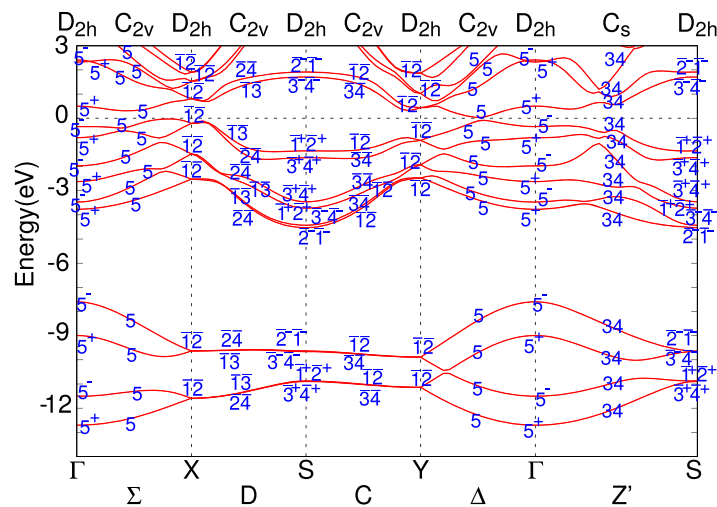


Fig. 5. (Color online) SOC band structure of non-buckled α bismuthene. The conventional IR are represented by numbers that correspond to the subscripts of Bethe symbols. The unconventional IR are represented by overlined numbers and their characters are shown in Table II. The superscript (\pm) indicates the parity.

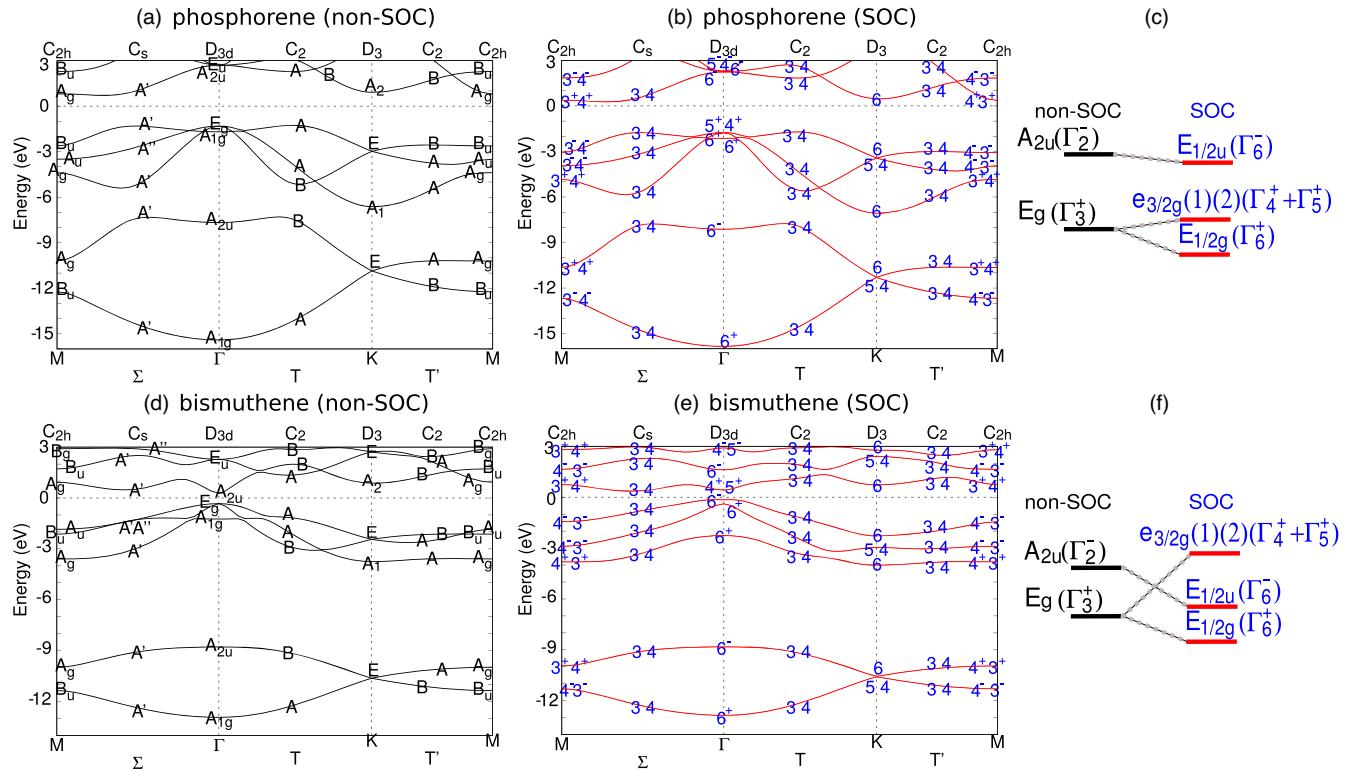


Fig. 6. (Color online) Non-SOC and SOC bands in the cases of β phosphorene [(a) and (b)] and β bismuthene [(d) and (e)]. Schematic views of the highest occupied and the lowest unoccupied bands at the Γ point in the cases of (c) phosphorene and (f) bismuthene are presented. In the non-SOC bands, the conventional IR are represented by Mulliken symbols. In the SOC bands, the conventional IR are represented by numbers which correspond to the subscripts of the Bethe symbols. The superscript (\pm) indicates the parities. In the case of the phosphorene SOC band, for example, 6^+ at the Γ point corresponds to Γ_6^+ .

We next carry out SOC calculations on β phosphorene [Fig. 6(b)]. Since the systems have the inversion symmetry, all the bands are degenerated due to Kramers pairing. At the Γ point, the valence band top belonging to E_g in the non-SOC band splits according to the direct product that $E_g(\Gamma_3^+) \otimes E_{1/2g}(\Gamma_6^+) = e_{3/2g}(1)(\Gamma_4^+) \oplus e_{3/2g}(2)(\Gamma_5^+) \oplus E_{1/2g}(\Gamma_6^+)$, where $E_{1/2g}(\Gamma_6^+)$ on the left-hand side is the IR of the spin functions. The original Mulliken notation $E_{3/2g}$ corresponds to two one-dimensional IR, Γ_4^+ and Γ_5^+ . Therefore, we introduce the symbols of $e_{3/2g}(1)$ and $e_{3/2g}(2)$ to represent Γ_4^+ and Γ_5^+ , respectively. The two bands belonging to these IR are degenerated due to the pairing originating from the time-reversal symmetry (Table III). On the other hand, $E_{1/2g}(\Gamma_6^+)$ is a two-dimensional IR. The numbers in the subscripts of E in the Mulliken symbols correspond to the magnetic quantum number of atomic spin-orbit wavefunctions. Therefore, it is natural that the $E_{1/2g}$ band is energetically lower than the $e_{3/2g}(1)$ and $e_{3/2g}(2)$ bands since the atomic spin-orbit function having the lower magnetic quantum number has lower energies.³⁵⁾ The non-SOC conduction band bottom belonging to A_{2u} corresponds to the SOC band belonging to $E_{1/2u}$ according to the direct product $A_{2u}(\Gamma_2^-) \otimes E_{1/2g}(\Gamma_6^+) = E_{1/2u}(\Gamma_6^-)$ as Fig. 6(c) shows. We find for α phosphorene that the energy difference between the $e_{3/2g}(1)(2)$ and $E_{1/2g}$ bands is very small (47 meV) because of a weak SOC. The energetical ascending order is $E_{1/2g}$, $e_{3/2g}(1)(2)$, and $E_{1/2u}$ [Fig. 6(c)].

The IR of the SOC band structure of β bismuthene are the same as those of β phosphorene except for the Γ point [Fig. 6(d)]. Since the SOC is strong in bismuthene, the split of E_g band at the Γ point is 800 meV and is much larger than

that (47 meV) in phosphorene. As a result, the $E_{1/2u}$ band originating from the non-SOC unoccupied A_{2u} band has a lower energy than the $e_{3/2g}(1)$ and $e_{3/2g}(2)$ bands originating from the non-SOC occupied E_g band. Due to this inversion of the energetical order, the highest occupied and the lowest unoccupied bands at the Γ point belong to and $E_{1/2u}$ and $e_{3/2g}(1)(2)$, respectively [Fig. 6(f)].

3.3. Z_2 invariant

We evaluate the topological invariants for systems having the inversion symmetry based on the group theoretical analysis. The Z_2 invariant ν is given by:^{48–52)}

$$(-1)^\nu = \prod_i \delta_i, \quad (7)$$

where i runs over the TRIM points. We calculate δ_i as follows:

$$\delta_i = \prod_{m=1}^{N_{occ}/2} \xi_{2m}(\mathbf{k}_i). \quad (8)$$

Here, $\xi_{2m}(\mathbf{k}_i)$ is the parity of the $2m$ -th band at the point \mathbf{k}_i . N_{occ} is the number of the occupied bands. $\nu = 1$ indicates that the system is a topological insulator.

We present ξ_{2m} in Tables IV and V for each band. We can judge the parity by analyzing Bethe (Mulliken) symbols where + and - (g and u) represent the parities of even and odd, respectively.

In the β structures, we consider the four TRIM points, Γ and three M points.^{35,48)} In the case of β phosphorene, we find that the highest occupied bands at the Γ point are paired. i.e. one-dimensional IR bands ($e_{3/2g}(1)$ and $e_{3/2g}(2)$) have the same energy and have the same parity of even. The other

Table IV. Analysis of Z_2 invariants in the case of β structures. ξ represents the parity of each band at a TRIM point in Eq. (8). The band number (N) in the ascending order of energy corresponds to m in Eq. (8).

β phosphorene				β bismuthene			
k -point	N	IR	ξ	k -point	N	IR	ξ
Γ (D_{3d})	5	$e_{3/2g}(1)(2) (\Gamma_4^+ \Gamma_5^+)$	+1	Γ (D_{3d})	5	$E_{1/2u} (\Gamma_6^-)$	-1
	4	$E_{1/2g} (\Gamma_6^+)$	+1		4	$E_{1/2g} (\Gamma_6^+)$	+1
	3	$E_{1/2g} (\Gamma_6^+)$	+1		3	$E_{1/2g} (\Gamma_6^+)$	+1
	2	$E_{1/2u} (\Gamma_6^-)$	-1		2	$E_{1/2u} (\Gamma_6^-)$	-1
	1	$E_{1/2g} (\Gamma_6^+)$	+1		1	$E_{1/2g} (\Gamma_6^+)$	+1
M (C_{2h})	5	$e_{1/2u}(1)(2) (M_{-3}^- M_4^-)$	-1	M (C_{2h})	5	$e_{1/2u}(1)(2) (M_{-3}^- M_4^-)$	-1
	4	$e_{1/2u}(1)(2) (M_{-3}^- M_4^-)$	-1		4	$e_{1/2u}(1)(2) (M_{-3}^- M_4^-)$	-1
	3	$e_{1/2g}(1)(2) (M_{+3}^+ M_4^+)$	+1		3	$e_{1/2g}(1)(2) (M_{+3}^+ M_4^+)$	+1
	2	$e_{1/2g}(1)(2) (M_{+3}^+ M_4^+)$	+1		2	$e_{1/2g}(1)(2) (M_{+3}^+ M_4^+)$	+1
	1	$e_{1/2u}(1)(2) (M_{-3}^- M_4^-)$	-1		1	$e_{1/2u}(1)(2) (M_{-3}^- M_4^-)$	-1

occupied bands at the Γ point belong to two-dimensional representations, i.e. $E_{1/2g}$ having the even parity or $E_{1/2u}$ having the odd parity. On the other hand, all the occupied bands at the M points belong to one-dimensional IR which are paired ($e_{1/2u}(1) (M_{-3}^-)$ and $e_{1/2u}(2) (M_{-4}^-)$ or $e_{1/2g}(1) (M_{+3}^+)$ and $e_{1/2g}(2) (M_{+4}^+)$ are paired) as Table III shows. By calculating Eqs. (7) and (8), we obtain that $\nu=0$ and this system is found to be a trivial insulator. This result is in contrast to group-IV materials which are found to be topological insulators.³⁵⁾

The parities of bands in the case of β bismuthene are the same as those of β phosphorene except for the highest occupied band at the Γ point (Table IV). As a result, $\nu=1$ in the case of β bismuthene, which is consistent with the result in the past studies.^{16,17,53)} The highest occupied bands at the Γ point belong to the two-dimensional IR of $E_{1/2u}$ and its

parity is odd in sharp contrast with the even parity in the case of β phosphorene (Table IV). As we have mentioned (in Sect. 3.2.2), the band of $E_{1/2u}$ originates from the lowest unoccupied non-SOC band of A_{2u} , which is due to the strong SOC that reverses the highest occupied and the lowest unoccupied bands (Fig. 6 (f)). Therefore, we conclude that the Z_2 invariant of 1 is due to the strong SOC in β bismuthene.

We next analyze the Z_2 invariants in the cases of non-buckled structures of α phosphorene and α bismuthene. Since both systems have the inversion symmetry, we can estimate the invariants by using Eqs. (7) and (8). The four TRIM points are Γ , X, S and Y points.⁵⁴⁾ Table V shows the parities of all occupied bands at these TRIM points. We find that the Kramers pairs at the Γ point belong to two-dimensional IR whereas the Kramers pairs at the S points belong to different one-dimensional IR having the same parity (Table V).

At the X (Y) point, two Kramers pairs have the same energy since the time-reversal symmetry causes the pairing of the unconventional two-dimensional IR, \bar{X}_1 and \bar{X}_2 (\bar{Y}_1 and \bar{Y}_2) (Table III). Since each two-dimensional IR includes the opposite parity, the quadruply degenerated bands contribute -1 to the product in Eq. (8). Therefore, based on the group theory, we can evaluate Eq. (8) without carrying out first-principles band calculations as for the X and Y points.

We find that $\nu=1$ in the case of unbuckled bismuthene, which is in sharp contrast with $\nu=0$ in the case of phosphorene and this result for the bismuthene is consistent with that of past studies.⁵⁴⁾ However, it was reported that the buckled structure which is the most stable for the free standing system has the value of $\nu=0$.¹⁷⁾ The non-buckled structure with $\nu=1$ is expected to be achieved when some substrates are used as was proposed in previous work.⁵⁴⁾

4. Conclusions

We carry out DFT calculations of group-V two-dimensional materials, phosphorene and bismuthene, and analyze the

Table V. Analysis of Z_2 invariants in the case of non-buckled α structures. ξ represents the parity of each band at a TRIM point in Eq. (8). The band number (N) in the ascending order of energy corresponds to m in Eq. (8).

α phosphorene					α bismuthene				
N	Γ (D_{2h})		S (D_{2h})		Γ (D_{2h})		S (D_{2h})		
	IR	ξ	IR	ξ	IR	ξ	IR	ξ	
10	$E_{1/2g} (\Gamma_5^+)$	+1	$\bar{S}_1^+ \bar{S}_2^+$	+1	$E_{1/2u} (\Gamma_5^-)$	-1	$\bar{S}_1^+ \bar{S}_2^+$	+1	
9	$E_{1/2g} (\Gamma_5^+)$	+1	$\bar{S}_3^+ \bar{S}_4^+$	+1	$E_{1/2g} (\Gamma_5^+)$	+1	$\bar{S}_3^+ \bar{S}_4^+$	+1	
8	$E_{1/2g} (\Gamma_5^+)$	+1	$\bar{S}_3^- \bar{S}_4^-$	-1	$E_{1/2u} (\Gamma_5^-)$	-1	$\bar{S}_3^- \bar{S}_4^-$	+1	
7	$E_{1/2u} (\Gamma_5^-)$	-1	$\bar{S}_1^- \bar{S}_2^-$	-1	$E_{1/2g} (\Gamma_5^+)$	+1	$\bar{S}_1^+ \bar{S}_2^+$	+1	
6	$E_{1/2u} (\Gamma_5^-)$	-1	$\bar{S}_3^+ \bar{S}_4^+$	+1	$E_{1/2u} (\Gamma_5^-)$	-1	$\bar{S}_3^- \bar{S}_4^-$	-1	
5	$E_{1/2u} (\Gamma_5^-)$	-1	$\bar{S}_1^+ \bar{S}_2^+$	+1	$E_{1/2g} (\Gamma_5^+)$	+1	$\bar{S}_1^- \bar{S}_2^-$	-1	
4	$E_{1/2g} (\Gamma_5^+)$	+1	$\bar{S}_1^- \bar{S}_2^-$	-1	$E_{1/2u} (\Gamma_5^-)$	-1	$\bar{S}_1^+ \bar{S}_2^+$	-1	
3	$E_{1/2g} (\Gamma_5^+)$	+1	$\bar{S}_3^- \bar{S}_4^-$	-1	$E_{1/2g} (\Gamma_5^+)$	+1	$\bar{S}_3^+ \bar{S}_4^+$	-1	
2	$E_{1/2u} (\Gamma_5^-)$	-1	$\bar{S}_1^+ \bar{S}_2^+$	+1	$E_{1/2u} (\Gamma_5^-)$	-1	$\bar{S}_1^- \bar{S}_2^-$	+1	
1	$E_{1/2g} (\Gamma_5^+)$	+1	$\bar{S}_3^+ \bar{S}_4^+$	+1	$E_{1/2g} (\Gamma_5^+)$	+1	$\bar{S}_3^- \bar{S}_4^-$	+1	
	X (D_{2h})		Y (D_{2h})		X (D_{2h})		Y (D_{2h})		
N	IR	ξ	IR	ξ	IR	ξ	IR	ξ	
9,10	$\bar{X}_1 \bar{X}_2$	-1	$\bar{Y}_1 \bar{Y}_2$	-1	$\bar{X}_1 \bar{X}_2$	-1	$\bar{Y}_1 \bar{Y}_2$	-1	
7,8	$\bar{X}_1 \bar{X}_2$	-1	$\bar{Y}_1 \bar{Y}_2$	-1	$\bar{X}_1 \bar{X}_2$	-1	$\bar{Y}_1 \bar{Y}_2$	-1	
5,6	$\bar{X}_1 \bar{X}_2$	-1	$\bar{Y}_1 \bar{Y}_2$	-1	$\bar{X}_1 \bar{X}_2$	-1	$\bar{Y}_1 \bar{Y}_2$	-1	
3,4	$\bar{X}_1 \bar{X}_2$	-1	$\bar{Y}_1 \bar{Y}_2$	-1	$\bar{X}_1 \bar{X}_2$	-1	$\bar{Y}_1 \bar{Y}_2$	-1	
1,2	$\bar{X}_1 \bar{X}_2$	-1	$\bar{Y}_1 \bar{Y}_2$	-1	$\bar{X}_1 \bar{X}_2$	-1	$\bar{Y}_1 \bar{Y}_2$	-1	

band structures based on the group theory. We identify IR of the calculated bands and consider sticking due to unconventional IR and pairing due to the time-reversal symmetry, which is beneficial for clarifying the origin of degeneracy.


Since α -structures are nonsymmorphic systems, we find some characteristic features of the band structures on the FBZE. Whereas the sticking and pairing induce double degeneracy for the non-SOC bands on the whole FBZE, the SOC induces a small amount of splitting in most cases. However, the X and Y points in the non-buckled structures are exceptional, i.e. the SOC bands are quadruply degenerated. Based on the identified IR, we find that the Z_2 invariant is 1 (0) in non-buckled α -bismuthene (α -phosphorene). In this analysis, we clarify that the quadruply degenerated bands at the X and Y points contribute to -1 in Eq. (8) based on the group theory.

We find that the Z_2 invariants are 0 and 1 in the cases of β -phosphorene and β -bismuthene, respectively. The origin of this difference between the two systems was clarified based on the group theory, i.e. the strong SOC reverses the highest occupied and the lowest unoccupied bands at the Γ point.

Acknowledgments

This work was partly supported by Grants-in-Aid for Scientific Research (No. 17K05118) from the Japan Society for the Promotion of Science (JSPS). Numerical calculations in this research were performed by using computer facilities at the Institute for Solid State Physics (ISSP) at the University of Tokyo.

ORCID iDs

Muhammad Yusuf Hakim Widiyanto  <https://orcid.org/0000-0002-1720-9754>

- 1) K. S. Novoselov, A. K. Geim, S. V. Morozov, D. Jiang, Y. Zhang, S. V. Dubonos, I. V. Grigorieva, and A. A. Firsov, *Science* **306**, 666 (2004).
- 2) A. Geim and K. Novoselov, *Nat. Mater.* **6**, 183 (2007).
- 3) P. Vogt, P. De Padova, C. Quaresima, J. Avila, E. Frantzeskakis, M. C. Asensio, A. Resta, B. Ealet, and G. Le Lay, *Phys. Rev. Lett.* **108**, 155501 (2012).
- 4) L. Li, Y. Yu, G. J. Ye, Q. Ge, X. Ou, H. Wu, D. Feng, H. Xian Chen, and Y. Zhang, *Nat. Nanotechnol.* **9**, 372 (2014).
- 5) M. N. Brunetti, O. L. Berman, and R. Y. Kezerashvili, *Phys. Rev. B* **100**, 155433 (2019).
- 6) Y. Tanaka, M. Saito, and F. Ishii, *Jpn. J. Appl. Phys.* **57**, 125201 (2018).
- 7) I. Žutić, J. Fabian, and S. Das Sarma, *Rev. Mod. Phys.* **76**, 323 (2004).
- 8) Z. Liu, C.-X. Liu, Y.-S. Wu, W.-H. Duan, F. Liu, and J. Wu, *Phys. Rev. Lett.* **107**, 136805 (2011).
- 9) T. Nagao, J. T. Sadowski, M. Saito, S. Yaginuma, Y. Fujikawa, T. Kogure, T. Ohno, Y. Hasegawa, S. Hasegawa, and T. Sakurai, *Phys. Rev. Lett.* **93**, 105501 (2004).
- 10) M. Saito, T. Ohno, and T. Miyazaki, *Appl. Surf. Sci.* **237**, 80 (2004).
- 11) S. Yaginuma, T. Nagao, J. Sadowski, M. Saito, K. Nagaoka, Y. Fujikawa, T. Sakurai, and T. Nakayama, *Surf. Sci.* **601**, 3593 (2007).
- 12) A. Takayama, T. Sato, S. Souma, and T. Takahashi, *Phys. Rev. Lett.* **106**, 166401 (2011).
- 13) T. Hirahara, T. Nagao, I. Matsuda, G. Bihlmayer, E. V. Chulkov, Y. M. Koroteev, P. M. Echenique, M. Saito, and S. Hasegawa, *Phys. Rev. Lett.* **97**, 146803 (2006).
- 14) H. Kotaka, F. Ishii, and M. Saito, *Jpn. J. Appl. Phys.* **52**, 035204 (2013).
- 15) T. Hirahara, G. Bihlmayer, Y. Sakamoto, M. Yamada, H. Miyazaki, S.-i. Kimura, S. Blügel, and S. Hasegawa, *Phys. Rev. Lett.* **107**, 166801 (2011).
- 16) S. Murakami, *Phys. Rev. Lett.* **97**, 236805 (2006).
- 17) M. Wada, S. Murakami, F. Freimuth, and G. Bihlmayer, *Phys. Rev. B* **83**, 121310 (2011).
- 18) M. Saito, Y. Takemori, T. Hashi, T. Nagao, and S. Yaginuma, *Jpn. J. Appl. Phys.* **46**, 7824 (2007).
- 19) H. Liu, A. T. Neal, Z. Zhu, Z. Luo, X. Xu, D. Tománek, and P. D. Ye, *ACS Nano* **8**, 4033 (2014).
- 20) J. Kang, J. D. Wood, S. A. Wells, J.-H. Lee, X. Liu, K.-S. Chen, and M. C. Hersam, *ACS Nano* **9**, 3596 (2015).
- 21) J. R. Brent, N. Savjani, E. A. Lewis, S. J. Haigh, D. J. Lewis, and P. O'Brien, *Chem. Commun.* **50**, 13338 (2014).
- 22) A. Castellanos-Gomez et al., *2D Mater.* **1**, 025001 (2014).
- 23) X. Liu, H. Bao, Y. Li, and Z. Yang, *Sci. Rep.* **10**, 21351 (2020).
- 24) T. Zhang, J.-H. Lin, Y.-M. Yu, X.-R. Chen, and W.-M. Liu, *Sci. Rep.* **5**, 13927 (2015).
- 25) A. Matsugatani, S. Ono, Y. Nomura, and H. Watanabe, *Comp. Phys. Commun.* **264**, 107948 (2021).
- 26) J. Gao, Q. Wu, C. Persson, and Z. Wang, *Comp. Phys. Commun.* **261**, 107760 (2021).
- 27) F. Tang, H. C. Po, A. Vishwanath, and X. Wan, *Nat. Phys.* **15**, 470 (2019).
- 28) M. G. Vergniory, L. Elcoro, C. Felser, N. Regnault, B. A. Bernevig, and Z. Wang, *Nature* **566**, 480 (2019).
- 29) T. Zhang, Y. Jiang, Z. Song, H. Huang, Y. He, Z. Fang, H. Weng, and C. Fang, *Nature* **566**, 475 (2019).
- 30) N. A. P. Namari and M. Saito, *Jpn. J. Appl. Phys.* **58**, 061003 (2019).
- 31) M. Y. H. Widiyanto, A. Zaharo, N. A. P. Namari, and M. Saito, *Jpn. J. Appl. Phys.* **60**, 061001 (2021).
- 32) S. Minami, I. Sugita, R. Tomita, H. Oshima, and M. Saito, *Jpn. J. Appl. Phys.* **56**, 105102 (2017).
- 33) M. Y. H. Widiyanto, H. P. Kadarisman, A. M. Yatmeidhy, and M. Saito, *Jpn. J. Appl. Phys.* **59**, 071001 (2020).
- 34) A. Zaharo, A. Purqon, T. Winata, and M. Saito, *Jpn. J. Appl. Phys.* **59**, 071006 (2020).
- 35) S. A. Putri, Y. Yamaguchi, T. A. Ariasoca, M. Y. H. Widiyanto, K. Tagami, and M. Saito, *Surf. Sci.* **714**, 121917 (2021).
- 36) T. Inui, Y. Tanabe, and Y. Onodera, *Group Theory and Its Applications in Physics* (Springer, Tokyo, 1990).
- 37) D. Vanderbilt, *Phys. Rev. B* **41**, 7892 (1990).
- 38) P. E. Blöchl, *Phys. Rev. B* **50**, 17953 (1994).
- 39) J. P. Perdew, K. Burke, and M. Ernzerhof, *Phys. Rev. Lett.* **77**, 3865 (1996).
- 40) T. Yamasaki, A. Kuroda, T. Kato, J. Nara, J. Koga, T. Uda, K. Minami, and T. Ohno, *Comput. Phys. Commun.* **244**, 264 (2019).
- 41) G. Koster, *Solid State Phys.* **5**, 173 (1957).
- 42) R. S. Mulliken, *J. Chem. Phys.* **23**, 1997 (1955).
- 43) R. S. Mulliken, *J. Chem. Phys.* **24**, 1118 (1956).
- 44) G. Herzberg, *Electronic Spectra and Electronic Structure of Polyatomic Molecules* (Van Nostrand, New York, 1966).
- 45) C. Herring, *Phys. Rev.* **52**, 361 (1937).
- 46) M. Kurpas, M. Gmitra, and J. Fabian, *Phys. Rev. B* **94**, 155423 (2016).
- 47) P. E. Faria Junior, M. Kurpas, M. Gmitra, and J. Fabian, *Phys. Rev. B* **100**, 115203 (2019).
- 48) L. Fu and C. L. Kane, *Phys. Rev. B* **76**, 045302 (2007).
- 49) L. Fu, C. L. Kane, and E. J. Mele, *Phys. Rev. Lett.* **98**, 10680 (2007).
- 50) Y. Kim, B. J. Wieder, C. L. Kane, and A. M. Rappe, *Phys. Rev. Lett.* **115**, 036806 (2015).
- 51) M. Z. Hasan and C. L. Kane, *Rev. Mod. Phys.* **82**, 3045 (2010).
- 52) C. L. Kane and E. J. Mele, *Phys. Rev. Lett.* **95**, 226801 (2005).
- 53) M. Gaffar, S. A. Wella, and E. H. Hasdeo, *Phys. Rev. B* **104**, 205105 (2021).
- 54) Y. Lu et al., *Nano Lett.* **15**, 80 (2015).